http://mmg.tversu.ru ISSN 2311-1275

Mathematical Modelling and Geometry

Volume 6, No 1, pp. 1 – 20 (2018) doi:10.26456/mmg/2018-611

How predictions of cosmological models depend on Hubble parameter data sets

G. S. Sharov and V. O. Vasiliev

Faculty of Mathematics, Tver State University, Sadovyi per. 35, Tver, Russia

e-mail: Sharov.GS@tversu.ru

Received 14 April 2018. Published 28 April 2018.

Abstract. We explore recent estimations of the Hubble parameter H depending on redshift z, which include 31 $H(z)$ data points measured from differential ages of galaxies and 26 data points, obtained with other methods. We describe these data together with Union 2.1 observations of Type Ia supernovae and observed parameters of baryon acoustic oscillations with 2 cosmological models: the standard cold dark matter model with the Λ term (ΛCDM) and the model with generalized Chaplygin gas (GCG). For these models with different sets of $H(z)$ data we calculate two-parameter and one-parameter distributions of χ^2 functions for all observed effects, estimate optimal values of model parameters and their 1σ errors. For both considered models the results appeared to be strongly depending on a choice of Hubble parameter data sets if we use all 57 $H(z)$ data points or only 31 data points from differential ages. This strong dependence can be explained in connection with 4 $H(z)$ data points with high redshifts $z > 2$.

Keywords: cosmological model, Chaplygin gas, Hubble parameter, Type Ia supernovae, baryon acoustic oscillations
MSC numbers: 83F05,83B05

1. Introduction

The latest astronomical observations and their astrophysical interpretation [1] let cosmologists conclude that our Universe demonstrates accelerated expansion and it contains $\simeq 4\%$ of visible baryonic matter, about 26% of cold dark matter and $\simeq 70\%$ of dark energy (DE). The visible and dark matter have properties of cold dust with close to zero pressure. However dark energy has another equation of state with large negative pressure p_{DE} close to its energy density $-\rho_{DE}$ with minus sign. Such a form of matter is considered as a source of the current cosmological acceleration, it helps us to construct a model that can describe all available now observational data and restrictions [1, 2, 3, 4].

The simplest way to modify the Einstein theory of gravitation and to include dark energy with the mentioned properties is to add the Λ term into the Einstein equations. In this case cosmological solutions can demonstrate accelerated expansion. The resulting dynamical equations may be also obtained, if we add the dark energy component with the equation of state $p_{DE} = -\rho_{DE}$ to the usual visible matter and cold dark matter components. This cosmological model is called ΛCDM (Λ term with cold dark matter), it is now the most popular and usually considered as the standard model in interpretation of observational data [1, 2, 3].

However, the ΛCDM model has some problems, in particular, vague nature of dark energy and dark matter, the fine tuning problem for the small observed value of Λ and the coincidence problem with surprising proximity of DE and matter contribution in total energy balance nowadays [5, 6]. Due to these reasons cosmologists suggest a lot of alternative models (see reviews [5, 6, 7]), in particular, scenarios with nontrivial equations of state [8, 9, 10, 11], with interaction between dark components [12, 13, 14, 15], with $F(R)$ Lagrangian [16, 17, 18], additional space dimensions [19] and many others.

In particular, in this paper together with the ΛCDM model we consider the model with generalized Chaplygin gas (GCG) [8, 9, 10, 11]. In this model two dark fluids — dark energy and dark matter are unified and represented as one dark component (generalized Chaplygin gas) with the following equation of state connecting energy density ρ_g and pressure p_g:

$$p_g = -B\,\rho_g^{-\alpha}. \tag{1}$$

Here B and α are positive constants. This fluid generalizes the classical Chaplygin gas [8] with the equation of state $p = \mathrm{const}/\rho$.

For the models ΛCDM and GCG in this paper we calculate limitations on model parameters determined from available recent observations including the Type Ia supernovae data (SN Ia) from Union 2.1 satellite [4], observable parameters baryon acoustic oscillations (BAO) and we pay special attention to different data sets of the Hubble parameter estimations $H(z)$.

Type Ia supernovae are usually considered as standard candles in the Universe, because they give possibility for each event to determine its epoch and the distance (luminosity distance) to this object. Supernova is an exploding star with huge

energy release, creating a shock wave on the expanding shell [20]. They are observed in rather far galaxies because of their giant luminosity. All supernovae are classified in correspondence with time dependence of the their brightness (the light curve) and their spectrum. In particular, stars of Type I have hydrogen-deficient optical spectrum and they belong to Type Ia subdivision, if they also have strong absorption near the silicon line 615 nm. For Type Ia supernovae astronomers can definitely determine their luminosity distances from light curves. In this paper Sect. 3 we use the Union 2.1 compilation [4] with 580 SN Ia.

The observable effect of baryon acoustic oscillations (BAO) is generated by acoustic waves with ions (baryons), which propagated in the relativistic plasma before the recombination epoch and stopped after the drag era corresponding to $z_d \simeq 1059.3$ [1]. This effect is observed as disturbances (a bump) in the correlation function of the galaxy distribution at the sound horizon scale $r_s(z_d)$ [1, 21]. In Sect. 3 we analyze two types of observational manifestations the BAO effect from Refs. [22] – [39], in particular, estimations of the Hubble parameter $H(z)$ for different redshifts z [28] – [39].

The Hubble parameter H is the logarithmic derivative of the scale factor a with respect to time t, redshift z is also expressed via a

$$H = \frac{\dot{a}}{a}, \qquad z = \frac{a_0}{a} - 1 = \frac{1}{a} - 1, \tag{2}$$

if we choose here and below the value a nowadays: $a_0 = a(t_0) = 1$.

The Hubble parameter $H(z)$ as the function of z may be estimated with different methods: in addition to the mentioned BAO effects [28] – [39] (26 data points) we also have the $H(z)$ data measured from differential ages of galaxies [40] – [46] (31 data points are tabulated Sect. 3).

In this paper we compare different approaches in choosing $H(z)$ data, make calculations with all 57 $H(z)$ data points or only 31 points from differential ages and demonstrate for 2 popular cosmological models ΛCDM and GCG that predictions of optimal model parameters strongly depend on a considered Hubble parameter data set.

In Sect. 2 we make a brief review of the models ΛCDM and GCG and their dynamics, in Sect. 3 describe observational data and in Sect. 4 we demonstrate and analyze the results of our calculations.

2. Models

For the ΛCDM model and the model with generalized Chaplygin gas (GCG) the dynamical equations are deduced from the Einstein equations for the Robertson-Walker metric with the curvature sign k

$$ds^2 = -dt^2 + a^2(t)\Big[(1 - kr^2)^{-1}dr^2 + r^2 d\Omega\Big]$$

and may be reduced to the system

$$3\frac{\dot{a}^2+k}{a^2} = 8\pi G\rho + \Lambda, \tag{3}$$

$$\dot{\rho} = -3\frac{\dot{a}}{a}(\rho + p). \tag{4}$$

Here the dot denotes the time derivative, ρ and p are correspondingly the energy density and pressure of all matter, G is the Newtonian gravitational constant, the constant Λ equals zero for the GCG model, the speed of light $c = 1$. Eq. (4) is the consequence of the continuity condition $\nabla_\mu T^\mu_\nu = 0$.

For both considered models we can neglect the fraction of relativistic matter (radiation and neutrinos), because the radiation-matter ratio is rather small $\rho_r/\rho_m \simeq 3 \cdot 10^{-4}$ [1] for observable values $z \leq 2.36$.

In the ΛCDM model baryons and dark matter may be considered as one component with density $\rho = \rho_b + \rho_{dm}$ that behaves like dust because of zero pressure $p = 0$. In this case we use the solution $\rho/\rho_0 = (a/a_0)^{-3}$ of Eq. (4) and rewrite the Friedmann equation (3) in the form

$$\frac{H^2}{H_0^2} = \Omega_m a^{-3} + \Omega_\Lambda + \Omega_k a^{-2} = \Omega_m(1+z)^3 + \Omega_\Lambda + \Omega_k(1+z)^2. \tag{5}$$

We divided Eq. (3) by $3H_0^2$, used Eq. (2) and the following notations for the present time fractions of matter, dark energy (Λ term) and curvature correspondingly:

$$\Omega_m = \frac{8\pi G\rho(t_0)}{3H_0^2}, \qquad \Omega_\Lambda = \frac{\Lambda}{3H_0^2}, \qquad \Omega_k = -\frac{k}{H_0^2}. \tag{6}$$

These values are connected by the equality

$$\Omega_m + \Omega_\Lambda + \Omega_k = 1, \tag{7}$$

resulting from Eq. (5) if we fix $t = t_0$. Thus, in description of the mentioned observational data the ΛCDM model has 3 independent parameters: H_0, Ω_m and Ω_Λ (or Ω_k).

The GCG model includes two matter components: baryons and the generalized Chaplygin gas, the common density is $\rho = \rho_b + \rho_g$. Unlike the ΛCDM in the GCG model one should separately consider baryonic matter (it may include some part of cold dark matter) and introduce the corresponding fraction

$$\Omega_b = \frac{8\pi G\rho_b(t_0)}{3H_0^2}$$

as an additional model parameter. However in Ref. [11] we demonstrated, that results of calculations very weakly depend on Ω_b. So in this paper we consider the simplified model with one (gas) component and suppose $\Omega_b = 0$ or $\rho = \rho_g$. In

this case one can substitute the equation of state (1) into Eq. (4), integrate it and obtain the following consequence of the Friedmann equation (3) [9, 10, 11]:

$$\frac{H^2}{H_0^2} = \Omega_k a^{-2} + (1-\Omega_k)\Big[B_s + (1-B_s)\,a^{-3(1+\alpha)}\Big]^{1/(1+\alpha)}. \tag{8}$$

Here the dimensionless parameter $B_s = B\rho_0^{-1-\alpha}$ is used instead of B. If we exclude the mentioned above parameter Ω_b, the GCG model will have 4 independent parameters: α, B_s, Ω_k and H_0.

3. Observational data

3.1 Supernovae Ia data

In Sect. 1 we briefly mentioned the observational data under investigation an here we describe details. For Type Ia Supernovae (SN Ia) we use $N_{SN} = 580$ data points from the table [4] after the Union 2.1 satellite investigation. This compilation provides observed (estimated) values of distance moduli $\mu_i = \mu_i^{obs}$ for redshifts z_i in the interval $0 < z_i \leq 1.41$. We fit free parameters of our models, when compare μ_i^{obs} with theoretical values $\mu^{th}(z_i)$ of the distance moduli, which are logarithms

$$\mu_i^{th} = \mu(D_L) = 5\log_{10}\big(D_L/10\text{pc}\big)$$

of the luminosity distance [1, 5]:

$$D_L(z) = \frac{c\,(1+z)}{H_0} S_k\left(H_0\int\limits_0^z \frac{d\tilde{z}}{H(\tilde{z})}\right), \quad S_k(x) = \begin{cases} \sinh\big(x\sqrt{\Omega_k}\big)/\sqrt{\Omega_k}, & \Omega_k > 0, \\ x, & \Omega_k = 0, \\ \sin\big(x\sqrt{|\Omega_k|}\big)/\sqrt{|\Omega_k|}, & \Omega_k < 0. \end{cases} \tag{9}$$

For a cosmological model with theoretical value $H(z)$ (5) or (8) depending on model parameters $p_1, p_2, \dots$ we calculate the distance $D_L(z)$ and the corresponding χ^2 function, that measures differences between the SN Ia observational data and predictions of a model:

$$\chi^2_{SN}(p_1, p_2, \dots) = \min_{H_0} \sum_{i,j=1}^{N_{SN}} \Delta\mu_i \big(C_{SN}^{-1}\big)_{ij} \Delta\mu_j, \tag{10}$$

where $\Delta\mu_i = \mu^{th}(z_i, p_1, \dots) - \mu_i^{obs}$, C_{SN} is the 580×580 covariance matrix [4]. For the Union 2.1 data [4] the standard marginalization over the nuisance parameter H_0 is required [11], it is made as the minimum over H_0 in the expression (10).

3.2 BAO data

For baryon acoustic oscillations (BAO) we take into account the values $d_z(z_i)$ [21]

$$d_z(z) = \frac{r_s(z_d)}{D_V(z)}, \qquad D_V(z) = \left[\frac{czD_L^2(z)}{(1+z)^2 H(z)}\right]^{1/3}. \tag{11}$$

They were extracted for redshifts (redshift ranges) $z = z_i$ from a peak in the correlation function of the galaxy distribution at the comoving sound horizon scale $r_s(z_d)$. The value z_d corresponds to decoupling of photons, for the sound horizon scale $r_s(z_d)$ here we use the following fitting formula [11]

$$r_s(z_d) = \frac{(r_d \cdot h)_{fid}}{h}, \qquad (r_d \cdot h)_{fid} = 104.57 \text{ Mpc}, \qquad h = \frac{H_0}{100 \text{ km/(s} \cdot \text{Mpc)}}, \quad (12)$$

providing true h dependence of r_d. The value $(r_d \cdot h)_{fid} = 104.57 \pm 1.44$ Mpc is the best fit for the ΛCDM model [11].

In our calculations we use $N_{BAO} = 26$ BAO data points for $d_z(z)$ (11) from Refs. [22] – [33], tabulated here in Table 1. We add 9 new points from Ref. [33] to 17 ones, which were used earlier in Refs. [10, 11, 14, 15, 18]. We use the covariance matrix C_d for correlated data from Refs. [22, 25] described in detail in Ref. [11]. So the χ^2 function for the value (11) yields

$$\chi^2_{BAO}(p_1, p_2, \dots) = \Delta d \cdot C_d^{-1} (\Delta d)^T, \qquad \Delta d_i = d_z^{obs}(z_i) - d_z^{th}(z_i). \quad (13)$$

Table 1: Values $d_z(z) = r_s(z_d)/D_V(z)$ (11) with errors and references

z	$d_z(z)$	σ_d	Refs	z	$d_z(z)$	σ_d	Refs
0.106	0.336	0.015	[24]	0.44	0.0916	0.0071	[25]
0.15	0.2232	0.0084	[27]	0.44	0.0874	0.0010	[33]
0.20	0.1905	0.0061	[22]	0.48	0.0816	0.0009	[33]
0.275	0.1390	0.0037	[22]	0.52	0.0786	0.0009	[33]
0.278	0.1394	0.0049	[23]	0.56	0.0741	0.0008	[33]
0.31	0.1222	0.0021	[33]	0.57	0.0739	0.0043	[29]
0.314	0.1239	0.0033	[25]	0.57	0.0726	0.0014	[32]
0.32	0.1181	0.0026	[32]	0.59	0.0711	0.0010	[33]
0.35	0.1097	0.0036	[22]	0.60	0.0726	0.0034	[25]
0.35	0.1126	0.0022	[26]	0.64	0.0675	0.0011	[33]
0.35	0.1161	0.0146	[28]	0.73	0.0592	0.0032	[25]
0.36	0.1053	0.0018	[33]	2.34	0.0320	0.0021	[31]
0.40	0.0949	0.0014	[33]	2.36	0.0329	0.0017	[30]

Unlike Refs. [11, 14, 15, 18] we do not use in this paper the observational value [21]

$$A(z) = \frac{H_0 \sqrt{\Omega_m}}{cz} D_V(z),$$

because it essentially depends on Ω_m, however Ω_m is not the model parameter for the GCG model (see Table 2).

3.3 $H(z)$ data

The Hubble parameter parameter values H at certain redshifts z can be measured with two methods: (1) extraction $H(z)$ from line-of-sight BAO data [28] – [39] including analysis of correlation functions of luminous red galaxies [28, 37], and (2) $H(z)$ estimations from differential ages Δt of galaxies (DA method) [40] – [46] via Eq. (2) and the following relation:

$$H(z) = \frac{\dot{a}}{a} = -\frac{1}{1+z}\frac{dz}{dt} \simeq -\frac{1}{1+z}\frac{\Delta z}{\Delta t}.$$

The maximal set with $N_H = 57$ recent estimations of $H(z)$ is shown in Fig. 1 and in Table 3 below, it includes 31 data points measured with DA method (the left side) and 26 data points (the right side), obtained with BAO and other methods. The χ^2 function for the $H(z)$ data is

$$\chi^2_H(p_1, p_2, \dots) = \sum_{i=1}^{N_H} \frac{\left[H_i - H^{th}(z_i, p_1, p_2, \dots)\right]^2}{\sigma^2_{H,i}}. \qquad (14)$$

In papers [14, 18] we used only $N_H = 30$ $H(z)$ data points estimated from DA method to avoid additional correlation with the BAO data from Table 1. This consideration should be taken into account in the present paper: in the next section we calculate separately the χ^2 function with $N_H = 31$ DA data points from the left column of Table 3 (30 points from Refs. [14, 18] and the recent point from Ref. [46]) and compare these results with the full $H(z)$ data from Table 3 with $N_H = 57$ data points.

In Fig. 1 the $H(z)$ data points from Table 3 estimated with DA and BAO methods are shown as correspondingly red stars and cyan diamonds. The lines demonstrate the best fitted $H(z)$ dependence with the optimal parameters from Table 2 for the ΛCDM and GCG models with 57 and 31 $H(z)$ data points.

4. Results of analysis

For any cosmological model we investigate the space of its model parameters $p_1, p_2, \dots$ (they are Ω_m, Ω_Λ, H_0 for the ΛCDM and α, B_s, Ω_k, H_0 for the GCG model) and search the optimal values of these parameters, which yield the most successful description of the observational data from Sect. 3. To achieve this purpose, for any set of parameters $p_1, p_2, \dots$ we use the dependence $H(z)$ (5) or (8), calculate the integral in Eq. (9), the distances $D_L = D^{th}_L(z)$ and $D^{th}_V(z)$ (11), the values μ^{th}, d^{th}_z, the χ^2 functions χ^2_{SN} (10), χ^2_{BAO} (13), χ^2_H (14) and the summarized function

$$\chi^2_{tot} = \chi^2_{SN} + \chi^2_{BAO} + \chi^2_H. \qquad (15)$$

We search minima of the functions χ^2_H and χ^2_{tot} in the parameter spaces of a model in the two mentioned variants of the $H(z)$ data sets: with all $N_H = 57$

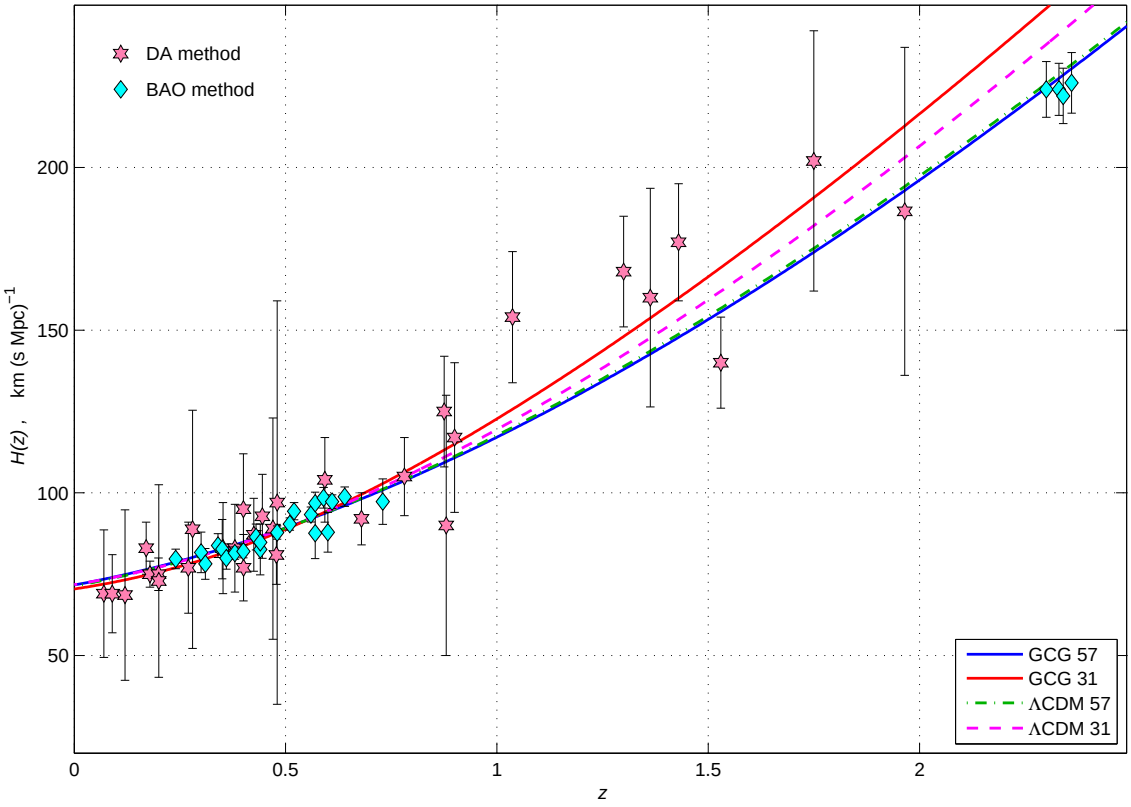

Figure 1: $H(z)$ data from Table 3, stars and diamonds denote data points correspondingly from DA and BAO methods. The lines are the best fitted for the ΛCDM and GCG models with 57 and 31 $H(z)$ data points.

data points from Table 3 and with only $N_H = 31$ data points from Refs. [40] – [46], estimated via the DA method.

For both considered models we calculate two-parameter distributions of $\min \chi^2_{tot}$ in planes of two model parameters, for example,

$$m^{\chi}_{tot}(p_1, p_2) = \min_{p_3,\dots} \chi^2_{tot}(p_1, p_2, p_3, \dots). \tag{16}$$

We use this functions to determine one-parameter distributions and the corresponding likelihood functions:

$$m^{\chi}_{tot}(p_j) = \min_{\text{other } p_k} \chi^2_{tot}(p_1, \dots), \qquad \mathcal{L}_{tot}(p_j) = \exp\left[-\frac{m^{\chi}_{tot}(p_j) - m_{abs}}{2}\right]. \tag{17}$$

Here m_{abs} is the absolute minimum of χ^2_{tot}.

The results of these calculations for the ΛCDM model with three independent parameters Ω_m, Ω_Λ and H_0 are presented in Figs. 2, 3 and in Table 2. In the

top-left panel of Fig. 2 we draw the contour plots at 1σ (68.27%), 2σ (95.45%) and 3σ (99.73%) confidence level for the two-parameter distributions (16) of χ^2_{tot} in the $(\Omega_m, \Omega_\Lambda)$ plane. The green filled contours describe the $m^{\chi}_{tot}(\Omega_m, \Omega_\Lambda)$ function for all 57 $H(z)$ data points, the magenta contours present the case with 31 DA $H(z)$ data points. Here the function (16) is

$$m^{\chi}_{tot}(\Omega_m, \Omega_\Lambda) = \min_{H_0} \chi^2_{tot}(\Omega_m, \Omega_\Lambda, H_0). \tag{18}$$

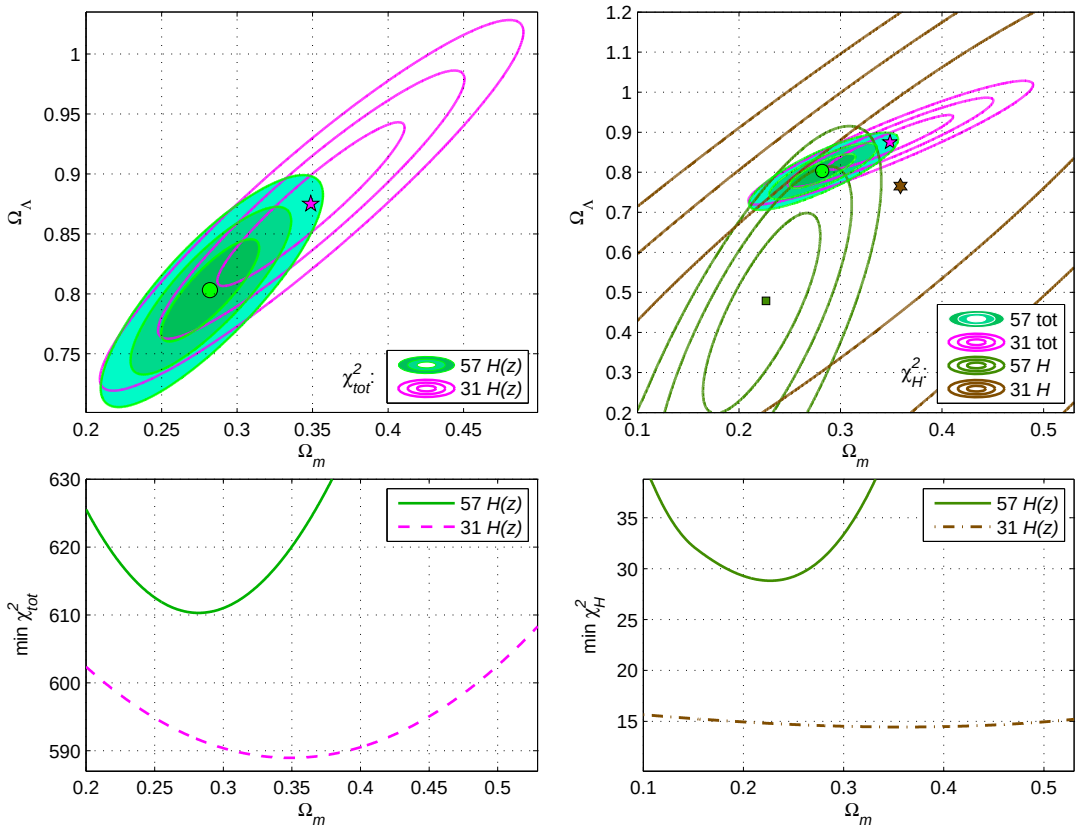

Figure 2: The ΛCDM model: 1σ, 2σ and 3σ contour plots for two-parameter distributions $m^{\chi}_{tot}(\Omega_m, \Omega_\Lambda)$ are drawn in $(\Omega_m, \Omega_\Lambda)$ plane for 57 and 31 $H(z)$ data points in comparison with contours for $\min\limits_{H_0} \chi^2_H$ (the top-right panel). The corresponding one-parameter distributions $m^{\chi}_{tot}(\Omega_m)$ and $m^{\chi}_H(\Omega_m)$ are in the bottom panels.

In the top-right panel of Fig. 2 we compare the mentioned contours for χ^2_{tot} (with the same colors) and the similar contours for the function χ^2_H (14), more correctly,

$$m^{\chi}_H(\Omega_m, \Omega_\Lambda) = \min_{H_0} \chi^2_H(\Omega_m, \Omega_\Lambda, H_0).$$

This distribution includes only $H(z)$ data.

The green circles and magenta stars in Fig. 2 denote the minimum points of $m^{\chi}_{tot}(\Omega_m, \Omega_\Lambda)$ (and, naturally, for χ^2_{tot}) correspondingly for 57 and 31 $H(z)$ data

points. Their coordinates (the optimal values of parameters) are tabulated in Table 2. In the same way, the minimum points for χ^2_H are shown in the top-right panel as the deep green square and brown hexagram.

In the bottom panels of Fig. 2 we compare the one-parameter distributions (17) $m^\chi_{tot}(\Omega_m)$ and $m^\chi_H(\Omega_m) = \min\limits_{\Omega_\Lambda} m^\chi_H(\Omega_m, \Omega_\Lambda)$. These distributions and the corresponding likelihood functions (17) determine 1σ estimates in Table 2 (for χ^2_{tot}).

In Fig. 2 we see the interesting phenomenon: the optimal values of parameters Ω_m, Ω_Λ (and positions of minimum points for χ^2) are essentially different for the two considered cases with 57 and 31 $H(z)$ data points. This divergence takes place for χ^2_{tot} (the left panels in Fig. 2), for example, these estimations for Ω_m are correspondingly $\Omega_m = 0.282 \pm 0.021$ and $\Omega_m = 0.349 \pm 0.041$ (see Table 2): the last value 0.349 is beyond 2σ confidence level for the $N_H = 57$ case. However for χ^2_H this divergence is stronger, the correspondent estimations are $\Omega_m = 0.227^{+0.036}_{-0.041}$ (for $N_H = 57$) and $\Omega_m = 0.359^{+0.197}_{-0.232}$ (for $N_H = 31$). This is natural, because the summands $\chi^2_{SN} + \chi^2_{BAO}$ in χ^2_{tot} moderate this effect.

Table 2: Optimal values and 1σ estimates of model parameters

Model	$\min \chi^2_{tot}$	AIC	H_0	Ω_k	other parameters
ΛCDM 57 $H(z)$	610.31	616.31	$71.35^{+0.63}_{-0.62}$	-0.085 ± 0.048	$\Omega_m = 0.282 \pm 0.021$, $\Omega_\Lambda = 0.803 \pm 0.028$
ΛCDM 31 $H(z)$	588.96	594.96	$71.77^{+1.70}_{-1.69}$	$-0.224^{+0.085}_{-0.084}$	$\Omega_m = 0.349 \pm 0.041$, $\Omega_\Lambda = 0.875 \pm 0.045$
GCG 57 $H(z)$	609.94	617.94	$71.68^{+0.82}_{-0.83}$	$-0.192^{+0.188}_{-0.170}$	$\alpha = -0.124^{+0.235}_{-0.138}$, $B_s = 0.705^{+0.065}_{-0.044}$
GCG 31 $H(z)$	587.93	595.93	$70.46^{+2.16}_{-2.51}$	$+0.019^{+0.541}_{-0.255}$	$\alpha = 0.647^{+3.25}_{-0.64}$, $B_s = 0.826^{+0.284}_{-0.111}$

Below we concentrate on the more relevant summarized function χ^2_{tot}. In Fig. 3 we present other two- and one-parameter distributions of χ^2_{tot} and the likelihood functions for the ΛCDM model. In particular, in the top-right panel the contour plots for $m^\chi_{tot}(\Omega_k, H_0) = \min\limits_{\Omega_m} \chi^2_{tot}$ are shown for the cases $N_H = 57$ and $N_H = 31$ in the same notations. In these calculation we consider the curvature fraction Ω_k as an independent parameter (together with Ω_m, H_0), the fraction Ω_Λ is expressed via Eq. (7): $\Omega_\Lambda = 1 - \Omega_m - \Omega_k$.

The two-parameter distributions (18) $m^\chi_{tot}(\Omega_m, \Omega_\Lambda)$ for $N_H = 57$ and 31 in the top-right panel of Figs. 2, 3 let us calculate the one-parameter distributions $m^\chi_{tot}(\Omega_m)$, $m^\chi_{tot}(\Omega_\Lambda)$ and the likelihood functions (17) $\mathcal{L}_{tot}(\Omega_m)$, $\mathcal{L}_{tot}(\Omega_\Lambda)$ shown in the middle and bottom panels of Fig. 3. The functions $\mathcal{L}_{tot}(H_0)$ are deduces from the two-parameter distributions in the (Ω_k, H_0) plane.

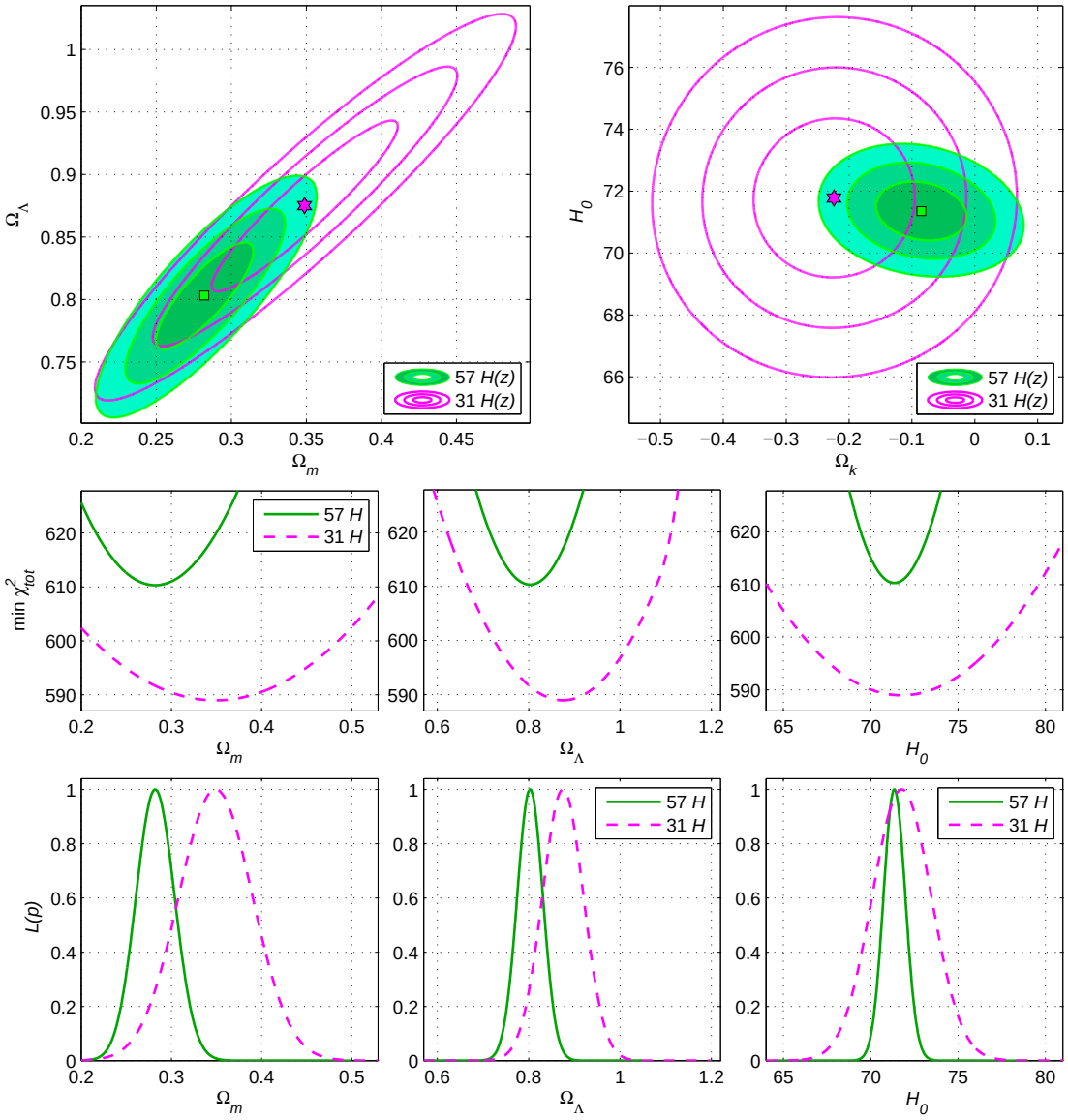

Figure 3: The ΛCDM model with 57 and 31 $H(z)$ data points: contour plots in 2 planes, one-parameter distributions and likelihood functions.

The best fitted values of $\min \chi^2_{tot}$ and the model parameters Ω_m, Ω_Λ, Ω_k, H_0 for the ΛCDM model are presented in Table 2 for the cases $N_H = 57$ and $N_H = 31$. The 1σ errors are calculated from the correspondent likelihood functions (17) $\mathcal{L}_{tot}(p_i)$. We should emphasize, that the number N_p of model parameters is essential, when we comrade different models. So we also use the Akaike information criterion [11, 47]

$$AIC = \min \chi^2_{tot} + 2N_p. \tag{19}$$

Here $N_p = 3$ for the ΛCDM model.

The similar estimations for the ΛCDM model were made in many papers, in particular, in Refs. [1, 2, 3, 11, 47, 48, 49] for describing the Type Ia supernovae, $H(z)$, BAO and other data in various combinations. One can observe the following

effect (connected with the described above): the estimations of Ω_m, Ω_Λ, Ω_k and H_0 in differen papers essentially depend a chosen $H(z)$ data set. For example, the authors of Refs. [49] used the χ^2_H function with $N_H = 41$ data points from both DA and BAO methods and calculated $\Omega_m = 0.237 \pm 0.051$, $\Omega_\Lambda = 0.66 \pm 0.20$. However, when they excluded 3 data points [30, 31, 36] with $z \geq 2.3$, they obtained the enhanced values for both parameters $\Omega_m = 0.40^{+0.18}_{-0.14}$, $\Omega_\Lambda = 0.92^{+0.34}_{-0.23}$ (compare with our results for χ^2_H in Fig. 2).

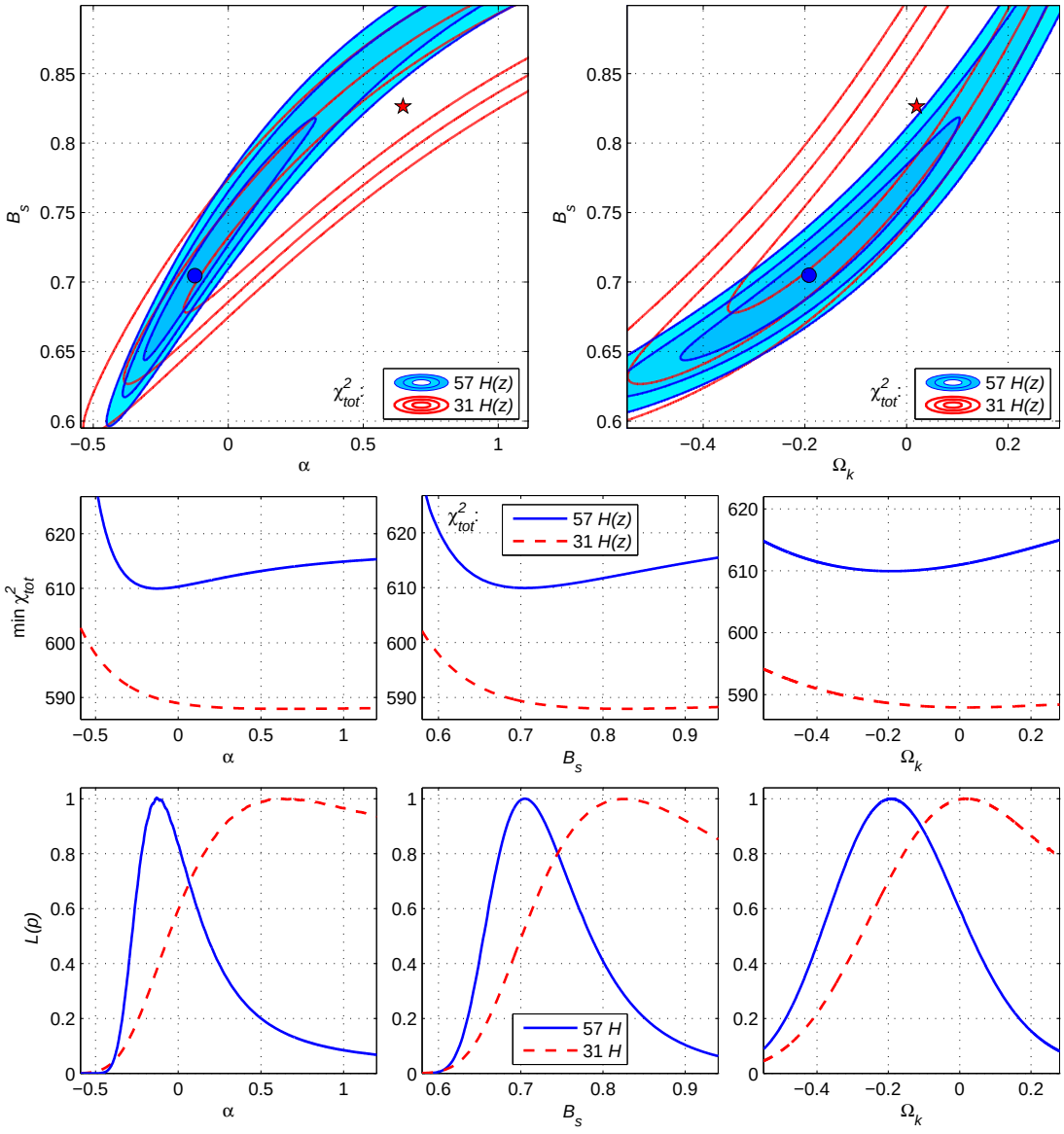

Figure 4: The GCG model with $N_H = 57$ (blue) and $N_H = 31$ (red): two-parameter, one-parameter distributions and likelihood functions for χ^2_{tot}.

If we compare our results for the ΛCDM model with the latest Planck data [1] ($\Omega_m = 0.308 \pm 0.012$, $\Omega_\Lambda = 0.692 \pm 0.012$, $\Omega_k = -0.005^{+0.016}_{-0.017}$, $H_0 = 67.8 \pm 0.9$

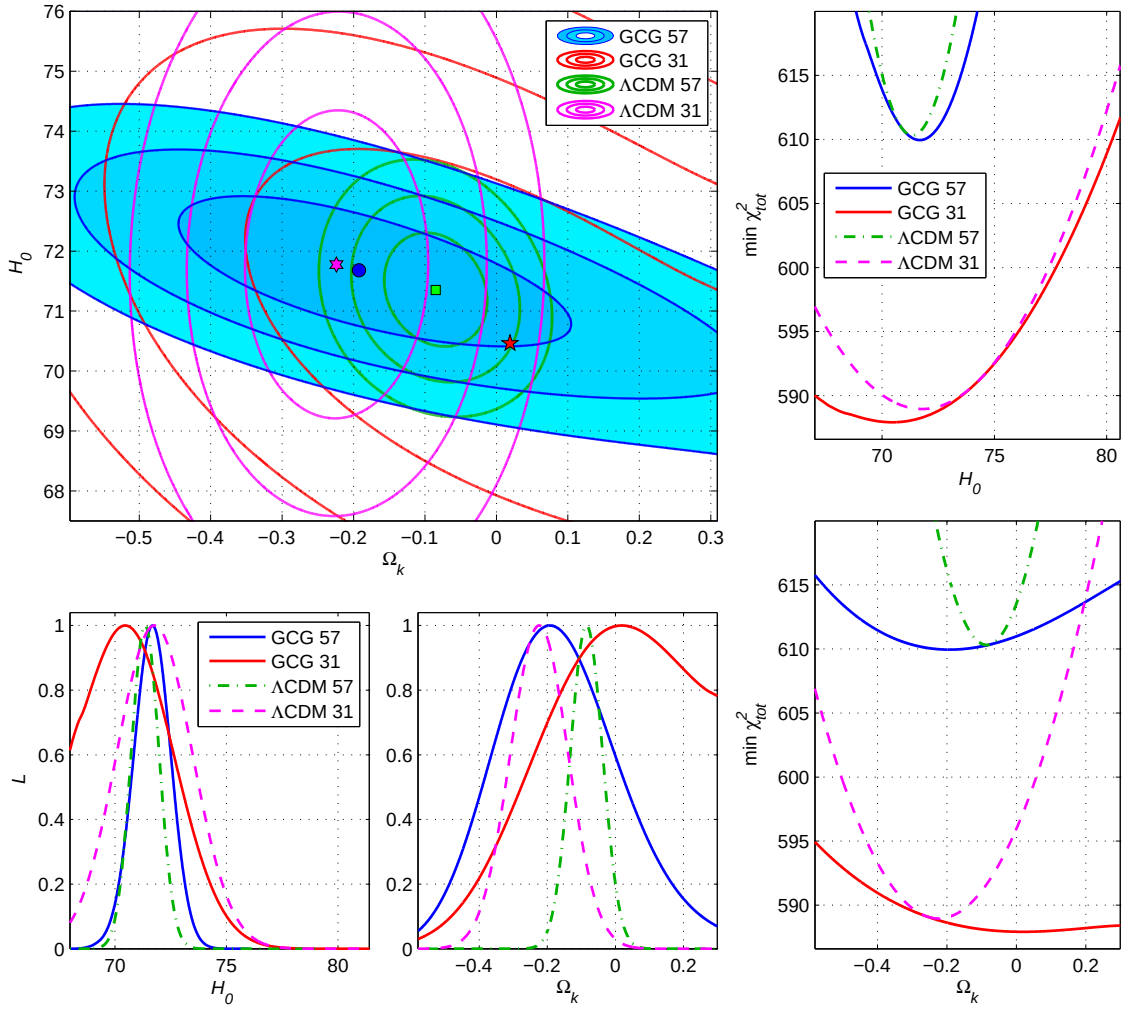

Figure 5: Comparison of the two-parameter distributions $\min \chi^2_{tot}(\Omega_k, H_0)$ for the ΛCDM and GCG models in the plane (Ω_k, H_0) of their common parameters for the cases with 57 and 31 $H(z)$ data points (the top-left panel). The corresponding one-parameter distributions are in other panels. Notations correspond to the previous figures.

km c^{-1}Mpc^{-1}), we will find some tension for Ω_Λ, $Omega_k$ in the case $N_H = 31$ and for H_0 in both cases because of too low estimation of H_0 in Ref. [1]).

The influence of a chosen $H(z)$ data set takes place not only for the ΛCDM model. One can see in Fig. 4 and in Table 2, that for the GCG model this influence is even more strong. In the top panels we demonstrate the contour plots for two-parameter distributions (16) of χ^2_{tot} in the (α, B_s) and (Ω_k, B_s) planes for the cases $N_H = 57$ (blue filled contours) and $N_H = 31$ (red contours). In particular, the two-parameter distributions (16) in the top-left panel are

$$m^{\chi}_{tot}(\alpha, B_s) = \min_{\Omega_k, H_0} \chi^2_{tot}(\alpha, B_s, \Omega_k, H_0).$$

The circles and stars show the points of minima for χ^2_{tot}. The similar two-parameter contour plots for the GCG model in the (Ω_k, H_0) plane are drawn in Fig. 5.

The one-parameter distributions $m^{\chi}_{tot}(\alpha)$, $m^{\chi}_{tot}(B_s)$, $m^{\chi}_{tot}(\Omega_k)$ and the corresponding likelihood functions (17) $\mathcal{L}_{tot}(p_i)$ are shown in the middle and bottom panels of Fig. 4.

Fig. 4 and Table 2 demonstrate, that for the GCG model the best fitted values of α, B_s, Ω_k strongly depend on a Hubble parameter data: $N_H = 57$ (all data points) or $N_H = 31$ (only from DA method). In part5icular, the best fitted values $\alpha \simeq -0.124$, $\Omega_k \simeq -0.192$ for $N_H = 57$ change their signs and become $\alpha \simeq +0.647$, $\Omega_k \simeq +0.019$, if $N_H = 31$.

In Fig. 5 we compare the ΛCDM and GCG models in the plane (Ω_k, H_0) of their common parameters. For both models we draw the one-parameter distributions $m^{\chi}_{tot}(\Omega_k)$, $m^{\chi}_{tot}(H_0)$ (they help us to compare the best results $\min \chi_{tot}$ for these models) and the likelihood functions $\mathcal{L}_{tot}(\Omega_k)$, $\mathcal{L}_{tot}(H_0)$.

In the top-left panel of Fig. 5 the filled contours describe the GCG model with $N_H = 57$, other contours differ in their color. The points of minima are marked here as the circle (GCG, $N_H = 57$), the pentagram (GCG, $N_H = 31$), the square (ΛCDM, $N_H = 57$) and the hexagrams (ΛCDM, $N_H = 31$) of the corresponding color.

Fig. 5 is useful, when we want to compare predictions the ΛCDM and GCG models in the considered cases $N_H = 57$ and $N_H = 31$. The plots $\mathcal{L}_{tot}(\Omega_k)$ and $\mathcal{L}_{tot}(H_0)$ show differences of the best fitted values, the plots $m^{\chi}_{tot}(\Omega_k)$ and $m^{\chi}_{tot}(H_0)$ describe effectiveness of these models. Mere detailed information is tabulated in Table 2.

5. Conclusion

In this paper we describe the observational data for Type Ia supernovae [4], BAO (Table 1) and two data sets of the Hubble parameter data $H(z)$ (all $N_H = 57$ data points from Table 3 and only 31 data points from differential ages) with the ΛCDM model and the model with generalized Chaplygin gas (GCG).

The results are demonstrated in Table 2: for all models and variants of N_H we calculated the minimal values of the function χ^2_{tot} (15), the results of Akaike information criterion (19) and the best fitted values of model parameters with 1σ errors. For the GCG model we achieve the best minimal values of $\min \chi^2_{tot}$, however the Akaike criterion gives advantage to the ΛCDM model, because it has the small number $N_p = 3$ of model parameters (degrees of freedom) in comparison with with $N_p = 4$ for GCG.

But the most striking result of our calculations for both models is the large difference between the best fitted values of model parameters in the cases with $N_H = 57$ $H(z)$ data points from Table 3 and $N_H = 31$ data points, obtained with DA method (the left hand side of Table 3). For the case $N_H = 57$ these results are close to the estimations for these models in Ref. [11], because in that paper we used $H(z)$ data points from both DA and BAO methods (though there were $N_H = 38$ points).

Table 3: Hubble parameter values $H(z)$ with errors σ_H from DA and BAO methods.

DA method				BAO method			
z	$H(z)$	σ_H	Refs	z	$H(z)$	σ_H	Refs
0.070	69	19.6	[42]	0.24	79.69	2.99	[34]
0.090	69	12	[40]	0.30	81.7	6.22	[37]
0.120	68.6	26.2	[42]	0.31	78.18	4.74	[33]
0.170	83	8	[40]	0.34	83.8	3.66	[34]
0.1791	75	4	[43]	0.35	82.7	9.1	[28]
0.1993	75	5	[43]	0.36	79.94	3.38	[33]
0.200	72.9	29.6	[42]	0.38	81.5	1.9	[38]
0.270	77	14	[40]	0.40	82.04	2.03	[33]
0.280	88.8	36.6	[42]	0.43	86.45	3.97	[34]
0.3519	83	14	[43]	0.44	82.6	7.8	[35]
0.3802	83	13.5	[45]	0.44	84.81	1.83	[33]
0.400	95	17	[40]	0.48	87.79	2.03	[33]
0.4004	77	10.2	[45]	0.51	90.4	1.9	[38]
0.4247	87.1	11.2	[45]	0.52	94.35	2.64	[33]
0.4497	92.8	12.9	[45]	0.56	93.34	2.3	[33]
0.470	89	34	[46]	0.57	87.6	7.8	[29]
0.4783	80.9	9	[45]	0.57	96.8	3.4	[32]
0.480	97	62	[41]	0.59	98.48	3.18	[33]
0.593	104	13	[43]	0.60	87.9	6.1	[35]
0.6797	92	8	[43]	0.61	97.3	2.1	[38]
0.7812	105	12	[43]	0.64	98.82	2.98	[33]
0.8754	125	17	[43]	0.73	97.3	7.0	[35]
0.880	90	40	[41]	2.30	224	8.6	[36]
0.900	117	23	[40]	2.33	224	8	[39]
1.037	154	20	[43]	2.34	222	8.5	[31]
1.300	168	17	[40]	2.36	226	9.3	[30]
1.363	160	33.6	[44]				
1.430	177	18	[40]				
1.530	140	14	[40]				
1.750	202	40	[40]				
1.965	186.5	50.4	[44]				

This essential divergence between the predictions of the variants with all $N_H = 57$ and $N_H = 31$ DA data points is seen visually in Fig. 1. It may be explained and connected with 4 $H(z)$ data points [30, 31, 36, 39] with high redshifts $z \geq 2.3$. These data points, obtained with BAO method (see the right hand side of Table 3) have small errors σ_H and strongly influence on a model predictions, when we take these points into account (in the case $N_H = 57$). Otherwise, when we include only $N_H = 31$ DA data points, this effect disappears.

References

[1] Planck Collaboration, Ade P.A.R. et al. *Planck 2015 results. XIII. Cosmological parameters.* Astron. Astrophys. 2016, **594**, A13, 66pp. (arXiv: 1502.01589)

[2] Ade P.A.R. et al. *Planck 2013 results. XVI. Cosmological parameters.* Astron. Astrophys. 2014, **571**, A16, 66pp. (arXiv: 1303.5076)

[3] Hinshaw G. et al. *Nine-year Wilkinson Microwave Anisotropy Probe (WMAP) Observations: Cosmological Parameters Results.* Astrophysical Journal Suppl. 2013, **208**, 19, 25pp. (arXiv: 1212.5226)

[4] Suzuki N. et al. *The Hubble Space Telescope Cluster Supernova Survey: V. Improving the Dark Energy Constraints Above $z > 1$ and Building an Early-Type-Hosted Supernova Sample.* Astrophys. J. 2012, **746**, 85, 24pp. (arXiv: 1105.3470);

[5] Clifton T., Ferreira P.G., A. Padilla and Skordis C. *Modified Gravity and Cosmology.* Physics Reports 2012, **513**, pp. 1 – 189 (arXiv: 1106.2476)

[6] Bamba K., Capozziello S., Nojiri S. and Odintsov S.D. *Dark energy cosmology: the equivalent description via different theoretical models and cosmography tests.* Astrophys. and Space Science 2012, **342**, pp. 155 – 228 (arXiv: 1205.3421)

[7] Nojiri S. and Odintsov S.D. *Unified cosmic history in modified gravity: from F(R) theory to Lorentz non-invariant models.* Physics Reports 2011, **505**, pp. 59 – 144 (arXiv: 1011.0544)

[8] Kamenshchik A.Y., Moschella U. and Pasquier V. *An alternative to quintessence.* Phys. Lett. B 2001, **511**, pp. 265 – 268 (arXiv: gr-qc/0103004)

[9] Bento M.C., Bertolami O. and Sen A.A. *Generalized Chaplygin gas, accelerated expans ion, and dark-energy-matter unification.* Phys. Rev. D **66**, pp. 043507, (arXiv: gr-qc/0202064)

[10] Sharov G.S. and Vorontsova E.G. *Parameters of cosmological models and recent astronomical observations.* J. Cosmol. Astropart. Phys. 2014, **10**, 057, 21pp. (arXiv: 1407.5405)

[11] Sharov G.S. *Observational constraints on cosmological models with Chaplygin gas and quadratic equation of state.* J. Cosmol. Astropart. Phys. 2016, **06** 023, 24pp. (arXiv: 1506.05246)

[12] Bolotin Yu.L., Kostenko A., Lemets O.A. and Yerokhin D.A. *Cosmological Evolution with Interaction Between Dark Energy and Dark Matter.* Int. J. Mod. Phys. D 2015, **24**, 1530007, 132pp. (arXiv: 1310.0085)

[13] Pan S., Bhattacharya S. and Chakraborty S. *An analytic model for interacting dark energy and its observational constraints.* Mon. Not. Roy. Astron. Soc. 2015, **452**, pp. 3038-3046 (arXiv: 1210.0396)

[14] Sharov G.S., Bhattacharya S., Pan S., Nunes R.C. and Chakraborty S. *A new interacting two fluid model and its consequences.* Mon. Not. Roy. Astron. Soc. 2017, **466**, pp. 3497-3506 (arXiv: 1701.00780)

[15] Pan S. and Sharov G.S. *A model with interaction of dark components and recent observational data.* Mon. Not. Roy. Astron. Soc. 2017, **472**, pp. 4736-4749 (arXiv: 1609.02287)

[16] Nojiri S. and Odintsov S.D. *Unifying inflation with LambdaCDM epoch in modified f(R) gravity consistent with Solar System tests.* Phys. Lett. B 2007, **657**, pp. 238 – 245 (arXiv: 0707.1941)

[17] E. Elizalde, Nojiri S., Odintsov S.D., L. Sebastiani and S. Zerbini. *Non-singular exponential gravity: a simple theory for early- and late-time accelerated expansion.* Phys. Rev. D 2011, **83** 086006, 22pp. (arXiv: 1012.2280)

[18] Odintsov S.D., Saez-Gomez D. and Sharov G.S. *Is exponential gravity a viable description for the whole cosmological history?* European Phys. J. C. 2017, **77**, 862, 17pp. (arXiv: 1709.06800)

[19] Grigorieva O.A. and Sharov G.S. *Multidimensional gravitational model with anisotropic pressure.* Intern. Journal of Modern Physics D 2013, **22**, 1350075 (arXiv: 1211.4992)

[20] Kirshner R.P. *Foundations of supernova cosmology.* In Dark Energy – Observational and Theoretical Approaches. Ed. Pilar Ruiz-Lapuente. 2010, 151pp. New York by Cambridge University Press (arXiv: 0910.0257)

[21] Eisenstein D.J. et al. *Detection of the baryon acoustic peak in the large-scale correlation function of SDSS luminous red galaxies.* Astrophys. J. 2005, **633**, pp. 560 – 574 (astro-ph/0501171)

[22] Percival W.J. et al.*Baryon acoustic oscillations in the Sloan Digital Sky Survey Data Release 7 galaxy sample.* Mon. Not. Roy. Astron. Soc. 2010, **401**, pp. 2148 – 2168 (arXiv: 0907.1660)

[23] Kazin E.A. et al. *The Baryonic Acoustic Feature and Large-Scale Clustering in the SDSS LRG Sample.* Astrophys. J. 2010, **710**, pp. 1444 – 1477 (arXiv: 0908.2598)

[24] Beutler F. et al., *The 6dF Galaxy Survey: Baryon Acoustic Oscillations and the Local Hubble Constant.* Mon. Not. Roy. Astron. Soc. 2011, **416**, pp. 3017 – 3032 (arXiv: 1106.3366)

[25] Blake C. et al. *The WiggleZ dark energy survey: mapping the distance redshift relation with baryon acoustic oscillations.* Mon. Not. Roy. Astron. Soc. 2011, **418**, pp. 1707 – 1724 (arXiv: 1108.2635)

[26] Padmanabhan N. et al. 2012, *A 2% Distance to* $z = 0.35$ *by Reconstructing Baryon Acoustic Oscillations - I : Methods and Application to the Sloan Digital Sky Survey.* Mon. Not. Roy. Astron. Soc. 2012, **427**, pp. 2132 – 2145 (arXiv: 1202.0090)

[27] Ross A.J. et al. *The Clustering of the SDSS DR7 Main Galaxy Sample I: A 4 per cent Distance Measure at* $z = 0.15$. 2015, **449**, pp. 835 – 847 (arXiv: 1409.3242)

[28] Chuang C.H. and Wang Y. *Modeling the Anisotropic Two-Point Galaxy Correlation Function on Small Scales and Improved Measurements of* $H(z)$, $D_A(z)$, *and* $f(z)\sigma_8(z)$ *from the Sloan Digital Sky Survey DR7 Luminous Red Galaxies.* Mon. Not. Roy. Astron. Soc. 2013, **435**, pp. 255 – 262 (arXiv: 1209.0210)

[29] Chuang C-H. et al. *The clustering of galaxies in the SDSS-III Baryon Oscillation Spectroscopic Survey: single-probe measurements and the strong power of* $f(z)\sigma_8(z)$ *on constraining dark energy.* Mon. Not. Roy. Astron. Soc. 2013, **433**, pp. 3559 – 3571 (arXiv: 1303.4486)

[30] Font-Ribera A. et al. *Quasar-Lyman* α *Forest Cross-Correlation from BOSS DR11: Baryon Acoustic Oscillations.* J. Cosmol. Astropart. Phys. 2014, **05**, 027, 26pp. (arXiv: 1311.1767)

[31] Delubac T. et al. *Baryon Acoustic Oscillations in the Ly*α *forest of BOSS DR11 quasars.* Astron. Astrophys. 2015, **574**, id. A59, 17 pp. 2014, 17pp. (arXiv: 1404.1801)

[32] Anderson L. et al. *The clustering of galaxies in the SDSS-III Baryon Oscillation Spectroscopic Survey: Baryon Acoustic Oscillations in the Data Release 10 and 11 Galaxy Samples.* Mon. Not. Roy. Astron. Soc. 2014, **441**, 24pp. (arXiv: 1312.4877)

[33] Wang Y. et al. *The clustering of galaxies in the completed SDSS-III Baryon Oscillation Spectroscopic Survey: tomographic BAO analysis of DR12 combined sample in configuration space.* Mon. Not. Roy. Astron. Soc. 2017, **469**, pp. 3762–3774 (arXiv: 1607.03154)

[34] Gaztañaga E., Cabre A., Hui L. *Clustering of Luminous Red Galaxies IV: Baryon Acoustic Peak in the Line-of-Sight Direction and a Direct Measurement of $H(z)$.* Mon. Not. Roy. Astron. Soc. 2009, **399**, pp. 1663 – 1680 (arXiv: 0807.3551)

[35] Blake C. et al. *The WiggleZ Dark Energy Survey: Joint measurements of the expansion and growth history at $z < 1$.* Mon. Not. Roy. Astron. Soc. 2012, **425**, pp. 405 – 414 (arXiv: 1204.3674)

[36] Busca N.G. et al. *Baryon Acoustic Oscillations in the Lyα forest of BOSS quasars.* Astron. and Astrop. 2013, **552**, A96, 18pp. (arXiv: 1211.2616)

[37] Oka A. et al. *Simultaneous constraints on the growth of structure and cosmic expansion from the multipole power spectra of the SDSS DR7 LRG sample.* Mon. Not. Roy. Astron. Soc. 2014, **439**, pp. 2515 – 2530 (arXiv: 1310.2820)

[38] Alam S. et al. *The clustering of galaxies in the completed SDSS-III Baryon Oscillation Spectroscopic Survey: cosmological analysis of the DR12 galaxy sample.* Mon. Not. Roy. Astron. Soc. 2017, **470**, pp. 2617–2652 (arXiv: 1607.03155)

[39] Bautista J. E. et al. *Measurement of baryon acoustic oscillation correlations at $z = 2.3$ with SDSS DR12 Lyα-Forests.* Astron. Astrophys. 2017, **603**, id. A12, 23pp. (arXiv: 1702.00176)

[40] Simon J., Verde L. and Jimenez R. *Constraints on the redshift dependence of the dark energy potential.* Phys. Rev. D 2005, **71**, 123001 (astro-ph/0412269)

[41] Stern D., Jimenez R., Verde L., Kamionkowski M. and Stanford S. A. *Cosmic chronometers: constraining the equation of state of dark energy. I: $H(z)$ measurements.* J. Cosmol. Astropart. Phys. 2010, **02**, 008pp. (arXiv: 0907.3149)

[42] Zhang C. et al. *Four New Observational H(z) Data From Luminous Red Galaxies Sloan Digital Sky Survey Data Release Seven.* Research in Astron. and Astrop. 2014, **14**, pp. 1221-1233 (arXiv: 1207.4541)

[43] Moresco M. et al. *Improved constraints on the expansion rate of the Universe up to z 1.1 from the spectroscopic evolution of cosmic chronometers.* J. Cosmol. Astropart. Phys. 2012, **8**, 006pp. (arXiv: 1201.3609)

[44] Moresco M. *Raising the bar: new constraints on the Hubble parameter with cosmic chronometers at $z \sim 2$.* Mon. Not. Roy. Astron. Soc.: Letters. 2015, **450**, pp. L16-L20 (arXiv: 1503.01116)

[45] Moresco M. et al. *A 6% measurement of the Hubble parameter at $z \sim 0.45$: direct evidence of the epoch of cosmic re-acceleration.* Journal of Cosmology and Astroparticle Physics. 2016, **05**, 014pp. (arXiv: 1601.01701)

[46] Ratsimbazafy A.L. et al. *Age-dating luminous red galaxies observed with the Southern African Large Telescope.* Mon. Not. Roy. Astron. Soc. 2017, **467**, pp. 3239–3254 (arXiv: 1702.00418)

[47] Shi K., Huang Y.F. and Lu T. *A comprehensive comparison of cosmological models from the latest observational data.* Monthly Notices Roy. Astronom. Soc. 2012, **426**, pp. 2452 – 2562 (arXiv: 1207.5875)

[48] Farooq O., Mania D. and Ratra B. *Hubble parameter measurement constraints on dark energy.* Astrophys. J. 2013, **764**, 138, 13 pp. (arXiv: 1211.4253)

[49] Jesus J.F., Gregorio T.M., Andrade-Oliveira F., Valentim R. and Matos C. A. O. *Bayesian correction of H(z) data uncertainties.* Mon. Not. Roy. Astron. Soc. 2018, **477**, pp. 2867 -– 2873 (arXiv: 1709.00646)